AIAA JOURNAL
Vol. 44, No. 3, March 2006

Numerical Study of Transonic Buffet on a Supercritical Airfoil

Q. Xiao* and H. M. Tsai†
National University of Singapore, Singapore 119260, Republic of Singapore
and
F. Liu‡
University of California, Irvine, Irvine, California 92697-3975

The flow of the Bauer–Garabedian–Korn (BGK) No. 1 supercritical airfoil is investigated by the solution of the unsteady Reynolds-averaged Navier–Stokes equations with a two-equation lagged k–ω turbulent model. Two steady cases ($M = 0.71$, $\alpha = 1.396$ deg and $M = 0.71$, $\alpha = 9.0$ deg) and one unsteady case ($M = 0.71$, $\alpha = 6.97$ deg), all with a far-stream Reynolds number of 20×10^6, are computed. The results are compared with available experimental data. The computed shock motion and the evolution of the concomitant flow separation are examined. Space-time correlations of the unsteady pressure field are used to calculate the time for pressure waves to travel downstream within the separated region from the shock wave to the airfoil trailing edge and then back from the trailing edge to the shock outside the separated region. The reduced frequency so calculated agrees well with the computed buffet frequency, supporting the signal propagation mechanism for buffet proposed by Lee (Lee, B. H. K., "Oscillation Shock Motion Caused by Transonic Shock Boundary-Layer Interaction," *AIAA Journal*, Vol. 28, No. 5, 1990, pp. 942–944).

Nomenclature

a	=	speed of sound
c	=	chord length
E	=	total energy
e	=	internal energy
k	=	turbulent mixing energy
M	=	Mach number
t	=	time
t^*	=	nondimensional time
U_∞	=	far-stream velocity
u_i	=	velocity vector
x_i	=	position vector
Pr	=	Prandtl number
Re	=	Reynolds number, $\rho U_\infty c/\mu$
α	=	angle of attack
β, β^*, σ, σ^*, ε, ε^*	=	turbulent closure coefficients
γ	=	ratio of specific heats
μ	=	dynamic viscosity
υ	=	kinematic viscosity
ρ	=	density
τ_{ij}, $\hat{\tau}_{ij}$	=	Reynolds and total stress tensors
ω	=	specific dissipation rate

Introduction

SELF-EXCITED oscillation has been investigated both experimentally and computationally since the early work of McDevitt et al.[1] (e.g., Refs. 1–19.) Previous experimental and numerical studies of transonic flow over an 18% thick circular-arc airfoil have indicated that the flow over a circular-arc airfoil exhibits varied behavior depending on the flow conditions. Three distinct regions of flight Mach number have been observed for a fixed freestream Reynolds number. Below a critical Mach number, the flow is steady and characterized by a weak shock wave near the midchord with trailing-edge flow separation. Above this critical Mach number, the flow becomes unsteady with unsteady shock motions on the upper and lower surfaces that are out of phase with each other. Shock-induced separation appears in the flow. As the Mach number is further increased, a steady shock reappears, and it is sufficiently strong to induce flow separation.

Compared to the nonlifting circular-arc airfoil, the study of lifting supercritical airfoils is at a lesser extent. Bartels[7] and Bartels et al.[8] reported computational and experimental studies of the NASASC(2)-0714 airfoil. An extensive set of data for the buffeting problem over the Bauer–Garabedian–Korn (BGK) No. 1 supercritical airfoil at transonic speeds was reported by Lee,[9] Lee et al.,[10] Lee,[11,12] and Lee et al.[13] The experiments were conducted over a range of Mach number and angle of attack. A map of the shock-induced trailing-edge separation regions together with steady and unsteady pressure measurements was reported for various shock/boundary-layer interactions. The investigation of supercritical airfoil indicates that, unlike the circular-arc airfoil, the supercritical airfoil has a much weaker trailing-edge separation and experiences only one-sided shock oscillation.

The mechanism of the self-excited oscillation is not well understood although the topic has been explored by several researchers.[11,13–19] The investigation on the biconvex airfoil suggests that the transonic periodic flows are initiated by an asymmetric unsteady disturbance. The shock-induced separation changes the effective geometry of the airfoil, which causes the forward and rearward movement of the shock depending on whether the streamtube decreases or increases. The necessary but not sufficient condition for the periodic flow to appear is that the shock wave be strong enough to cause boundary-layer separation. The Mach number just upstream of the shock should be in the range between 1.14 and 1.24. For the supercritical airfoil,[11] a model to predict the shock motion was formulated. The model assumes that the movement of the shock leads to the formation of pressure waves which propagate downstream within the separated flow region. On reaching the trailing edge, the disturbance generates upstream-moving waves, which interact with the shock wave and impart energy to maintain the limit cycle. Unlike the downstream waves, the upstream-moving waves travel in the region outside the separated boundary layer. The period of the oscillation should be the time for a disturbance to propagate from shock to the trailing edge plus the duration for an upstream moving wave to reach the shock from the trailing edge. No computational

Received 16 March 2005; revision received 7 September 2005; accepted for publication 7 September 2005.

*Research Scientist, Temasek Laboratories.
†Principal Research Scientist, Temasek Laboratories. Member AIAA.
‡Professor, Department of Mechanical and Aerospace Engineering. Associate Fellow AIAA.

work of buffeting flow for this class of airfoils has been reported to the authors' knowledge.

In this paper, we present computational results of buffeting flow over the BGK No. 1 supercritical airfoil as studied experimentally by Lee,[9] Lee et al.,[10] and Lee.[11,12] The computations are performed by a finite volume method for the unsteady Reynolds-averaged Navier–Stokes equations using a lagged k–ω model.[20,21] The lagged model proposed by Olsen and Coakley[22] is used to remedy the inadequacy of the baseline k–ω model in dealing with nonequilibrium turbulent flow, which is often the case for unsteady flow involving shock-boundary-layer interaction. Self-excited oscillations of the flow over the BGK No. 1 airfoil are reproduced computationally by this method. The computational results are compared with the experimental data. Spatial correlations and Fourier transforms of the unsteady disturbances inside and outside the separated boundary layer in the region between the shock wave and airfoil trailing edge are examined to confirm the proposed mechanism by Lee et al. In the next section, the lagged k–ω turbulence model along with the numerical method is outlined. Computational results and discussions will then be presented. Finally, conclusions are drawn based on the results.

Numerical Method

The governing equations for the unsteady compressible turbulent flow are expressed as follows.

Mass conservation:

$$\frac{\partial \rho}{\partial t} + \frac{\partial}{\partial x_j}(\rho u_j) = 0 \tag{1}$$

Momentum conservation:

$$\frac{\partial}{\partial t}(\rho u_i) + \frac{\partial}{\partial x_j}(\rho u_j u_i) = -\frac{\partial p}{\partial x_i} + \frac{\partial \hat{\tau}_{ji}}{\partial x_j} \tag{2}$$

Mean energy conservation:

$$\frac{\partial}{\partial t}(\rho E) + \frac{\partial}{\partial x_j}(\rho u_j H) = \frac{\partial}{\partial x_j}\left[u_i \hat{\tau}_{ij} + (\mu + \sigma^* \mu_T)\frac{\partial k}{\partial x_j} - q_j\right] \tag{3}$$

Turbulent mixing energy:

$$\frac{\partial}{\partial t}(\rho k) + \frac{\partial}{\partial x_j}(\rho u_j k) = \tau_{ij}\frac{\partial u_i}{\partial x_j} - \beta^* \rho \omega k + \frac{\partial}{\partial x_j}\left[(\mu + \sigma^* \mu_T)\frac{\partial k}{\partial x_j}\right] \tag{4}$$

Specific dissipation rate:

$$\frac{\partial}{\partial t}(\rho \omega) + \frac{\partial}{\partial x_j}(\rho u_j \omega) = \left(\frac{\varepsilon \omega}{k}\right)\tau_{ij}\frac{\partial u_i}{\partial x_j} - \beta \rho \omega^2 + \frac{\partial}{\partial x_j}\left[(\mu + \sigma \mu_T)\frac{\partial \omega}{\partial x_j}\right] \tag{5}$$

Turbulent eddy viscosity:

$$\frac{\partial}{\partial t}(\rho v_t) + \frac{\partial}{\partial x_j}(\rho u_j v_t) = a(R_T)\omega \rho (v_{\mathrm{tE}} - v_t) \tag{6}$$

The total energy and enthalpy are $E = e + k + u_i u_i/2$ and $H = h + k + u_i u_i/2$, respectively, with $h = e + p/\rho$ and $e = p/[(\gamma - 1)\rho]$. Other quantities are defined in the following equations:

$$\mu_T = \rho v_t \tag{7}$$

$$v_{\mathrm{tE}} = \frac{\varepsilon^* k}{\omega} \tag{8}$$

$$R_T = \frac{\rho k}{\mu_T \omega} \tag{9}$$

$$S_{ij} = \frac{1}{2}\left(\frac{\partial u_i}{\partial x_j} + \frac{\partial u_j}{\partial x_i}\right) \tag{10}$$

$$\tau_{ij} = 2\mu_T\left(S_{ij} - \frac{1}{3}\frac{\partial u_k}{\partial x_k}\delta_{ij}\right) - \frac{2}{3}\rho k \delta_{ij} \tag{11}$$

$$\hat{\tau}_{ij} = 2\mu\left(S_{ij} - \frac{1}{3}\frac{\partial u_k}{\partial x_k}\delta_{ij}\right) + \tau_{ij} \tag{12}$$

$$q_j = -\left(\frac{\mu}{Pr_L} + \frac{\mu_T}{Pr_T}\right)\frac{\partial h}{\partial x_j} \tag{13}$$

$$a(R_T) = a_0\left[\frac{(R_T + R_{T0})}{(R_T + R_{T\infty})}\right] \tag{14}$$

The other coefficients are as follows:

$$a_0 = 0.35, \qquad R_{T0} = 1, \qquad R_{T\infty} = 0.01$$

$$\varepsilon = 5/9, \qquad \varepsilon^* = 1, \qquad \beta = 0.075$$

$$\beta^* = 0.09, \qquad \sigma = 0.5, \qquad \sigma^* = 0.5$$

The validity of turbulence models for unsteady flows featuring buffet and/or dynamic stall has received much attention lately. In the early work of Levy,[2] computations were done using the Baldwin–Lomax[23] model. Algebraic turbulence models such as the Baldwin–Lomax model do not perform well for flows with large separations (see Ref. 14). Barakos and Drikakis[6] recently presented an assessment of more advanced turbulence closures for transonic buffeting flows over airfoils. Various turbulence closures such as the algebraic model, the one-equation model of Spalart and Allmaras,[24] the Launder–Sharma[25] and Nagano–Kim[26] linear k–ε models, the nonlinear eddy-viscosity model of Craft et al.,[27] and the nonlinear k–ω model of Sofialidis and Prinos[28] were studied with limited success. One difficulty in most turbulence models is the inability to account directly for nonequilibrium effects found in separated flows. The conventional one- and two-equation turbulence models generate Reynolds stresses that respond too rapidly to changes in mean flow conditions partially because of the need to accurately reproduce equilibrium flows. As a result, these baseline turbulence models give unsatisfactory results for flows with significant separation under adverse pressure gradients or across shock waves. In the preceding formulation, the standard k–ω turbulence model is coupled with the lag model proposed by Olsen and Coakley[22] to calculate the turbulent eddy viscosity. The basic idea of the lag model is to take a baseline two-equation model Eqs. (4) and (5) and couple it with a third (lag) equation (6) to model the nonequilibrium effects for the eddy viscosity. Xiao et al.[20] incorporated the lag model with the baseline k–ω model and computed both steady and unsteady transonic nozzle flows. Their computations show notable improvements for strong shock cases, where strong nonequilibrium effect is present.

The basic numerical method used to solve the preceding system of equations is described in Xiao et al.[20] and Liu and Ji.[29] The integral forms of the conservation equations are discretized on quadrilateral cells using the finite volume approach. A staggered scheme is used for the coupling of Navier–Stokes equations and the k–ω and lag equations. A central difference scheme is used to discretize the diffusive terms, and a second-order upwind Roe's scheme is used for convective terms in the Navier–Stokes and the k–ω equations. After being discretized in space, the governing equations are reduced to a set of ordinary differential equations with only derivatives in time, which can be solved using a multistage Runge–Kutta-type scheme. The dual time-stepping method is adopted here for time marching. To accelerate the convergence, the unsteady multigrid method proposed by Jameson[30] and further implemented by Liu and Ji[29] is applied in the present study for all seven equations.

Computational Results and Discussion

The numerical method just presented is applied to the BGK No. 1 supercritical airfoil, which is extensively investigated experimentally by Lee and coworkers.[9–13] The geometry of the airfoil is shown

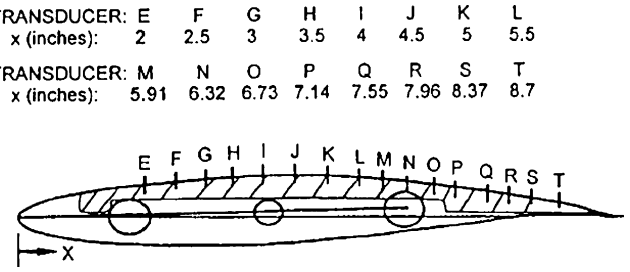

Fig. 1 Geometry of the BGK No. 1 supercritical airfoil (from Ref. 9).

in Fig. 1. The experiments have been conducted at a chord Reynolds number of 20×10^6 with free transition. The Mach numbers in the investigation ranged from 0.5 to 0.792 with the angle of attack α varying from 1.3 to 11.5 deg. Based on the measured force and pressure power spectrum, strong shock oscillation are observed for Mach numbers between 0.69 and 0.733. For the present numerical simulation, three test cases are investigated with a fixed chord Reynolds number of 20×10^6 and Mach number of 0.71 at three different angles of attack; case 1, $\alpha = 1.396$ deg; case 2, $\alpha = 6.97$ deg; and case 3, $\alpha = 9.0$ deg. Based on Lee's experimental results, the flow is steady for the flow conditions of cases 1 and 3. For case 2, however, the flow is unsteady with shock-induced oscillation.

The computations are performed by the following procedure. Starting from the initial field, the flowfield solution is integrated in time by using the dual-time-stepping method. The physical time step, nondimensionalized by the freestream speed and chord length is 0.05. After the initial development of the solution, the flow can achieve a quasi-steady periodic condition, monitored by the time history of the lift coefficient on the airfoil. Once the flow achieves a periodic state, the lift coefficient and pressure distribution along the airfoil are sampled at every iteration. A fast Fourier transform (FFT) of the lift coefficient is then performed and the dominant frequencies identified. The code is usually run for a length of 150 to 200 nondimensional time (tU_∞/c) to allow the solutions to become periodic. All three cases are computed using three levels of multigrids with a Courant–Friedrichs–Lewy number in the range between 3.0 and 7.0.

The computational grid has a C-topology. Most of the computations are performed on a 640×64 mesh with 512 points on the surface of airfoil, 128 nodes in the wake. The computational domain extends approximately 20 chords up- and downstream. The average minimum normal spacing at the wall is approximately 10^{-6} chord, which corresponds to a y^+ value of about 0.6 for an unsteady calculation at $M = 0.71$ with $\alpha = 6.97$ deg. The no-slip boundary conditions are imposed on the airfoil surface. At the outer boundary, far-field Riemann invariant boundary conditions are employed, and at the downstream all variables are extrapolated. A mesh independence study is conducted for the unsteady calculation at $M = 0.71$ with $\alpha = 6.97$ deg. The fine grid has 960×96 points, the medium 640×64, and the coarse grid 320×32. Time history of the lift coefficient, oscillation reduced frequency (defined as $k = \pi f c/U_\infty$), and time-mean pressure distribution on the three meshes are compared to one another. Figures are omitted to save space. It suffices to summarize that large discrepancies exist between the solution on the coarse grid and those on the finer grids for the time history of Cl and the pressure distributions, although the predominant reduced frequency (0.16) is not sensitive to the grid. This indicates that the 320×32 grid is not sufficient to correctly predict the flowfield. For the medium and fine grid, the difference in pressure coefficient distribution is small except the shock captured by the fine-grid solution appears to be sharper than that by the medium grid and closer to the experiment. The computational results presented in the following are obtained on the 640×64 grid.

As the initial conditions are different in the experiments and the computations, it is important to investigate their influence on the characteristics of the computed unsteady buffeting flows. Two test cases are carried out for $M = 0.71$ and $\alpha = 6.97$ deg. One starts from a uniform flow, and the other starts from a convergent steady solution for $M = 0.71$ and $\alpha = 1.396$ deg. Computations reveal that the time for the flow to reach a periodic solution is earlier for the calculation initialized with the convergent steady result. But once the periodic state is reached, the time-mean lift coefficient and the oscillation amplitude and frequency are found to be the same for the two cases. The time-mean pressure distributions are also the same.

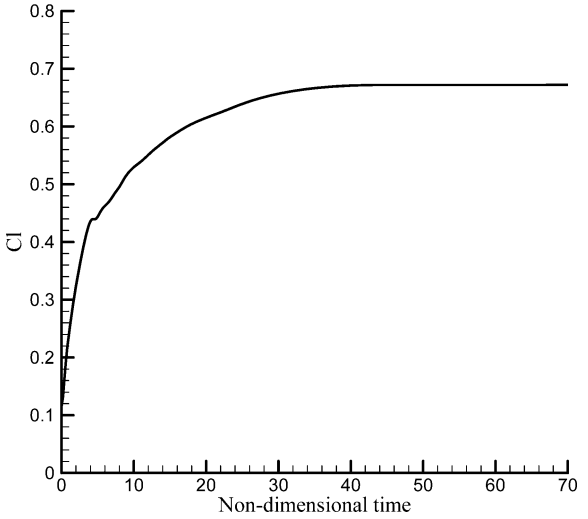

Fig. 2 Evolution of lift coefficient Cl of $M = 0.71$ and $\alpha = 1.30$ deg.

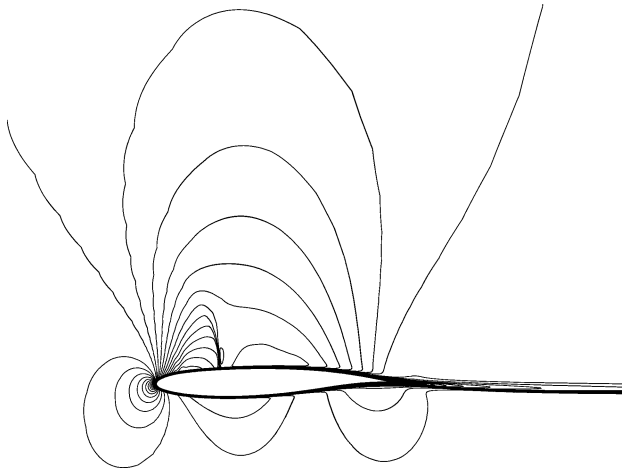

Fig. 3 Mach contour of $M = 0.71$ and $\alpha = 1.30$ deg; $\Delta M = 0.077$.

Case 1 ($M = 0.71$, $\alpha = 1.396$ deg)

The experimental data for case 1 are $M = 0.71$ and $\alpha = 1.396$ deg; however, the computations use $M = 0.71$, $\alpha = 1.30$ deg to account for wind-tunnel corrections. The time-accurate evolution of the lift coefficient Cl is shown in Fig. 2 with the computation starting from the uniform freestream flow. The computed Cl eventually approaches a constant around 0.66, which indicates that the flow is steady without shock-induced oscillations. The Mach contours shown in Fig. 3 reveal a weak shock formed at about one quarter-chord of the airfoil without flow separation. The pressure coefficient distribution along the airfoil upper surface is shown in Fig. 4 as well as the experimental data of Lee et al.[10] and the computational result obtained with the original experimental angle of attack. The computation with the corrected angle of attack is closer to the experiment. An overly downstream shock location is predicted by the result without the correction.

Case 2 ($M = 0.71$, $\alpha = 6.97$ deg)

The lift coefficient Cl evolution is presented in Fig. 5. The flow at this condition develops into an unsteady mode with shock-induced oscillation. The average lift coefficient is 1.03, which is close to the experimental data of 1.016. Fourier analysis of the lift coefficient shown in Fig. 6 reveals a predominant reduced frequency of 0.16.

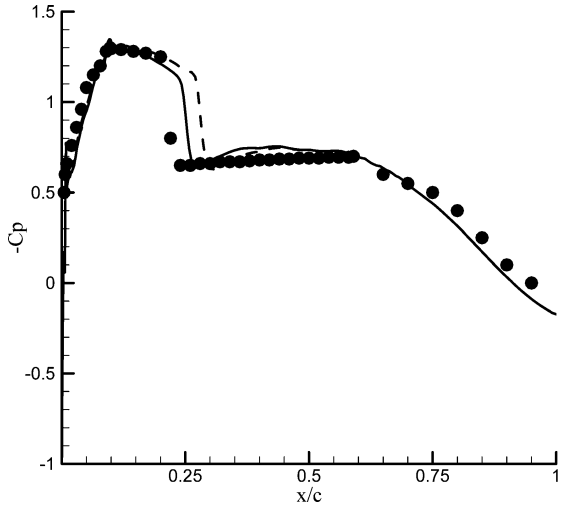

Fig. 4 Pressure comparison with experimental results: ●, experiment; ——, computation for $M = 0.71$, $\alpha = 1.30$ deg; and – – –, computation for $M = 0.71$ and $\alpha = 1.396$ deg.

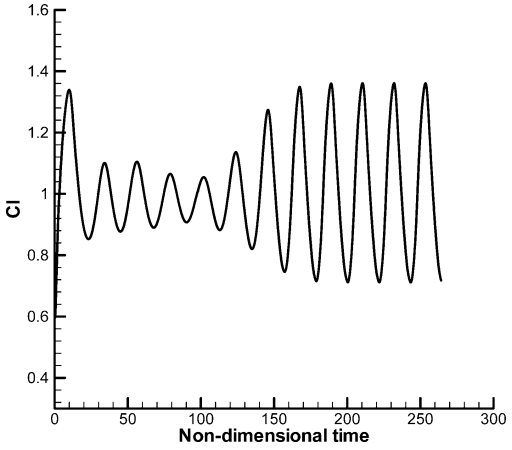

Fig. 5 Evolution of lift coefficient Cl of $M = 0.71$ and $\alpha = 6.97$ deg.

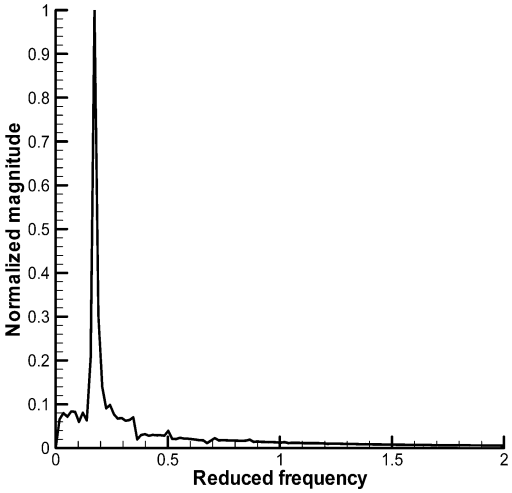

Fig. 6 Fourier analysis of reduced frequency for $M = 0.71$ and $\alpha = 6.97$ deg.

This value is about 36% lower than the experiment of Lee et al.[10] ($k = \pi f c / U_\infty = 0.25$). The same code was used for the computation of the buffeting phenomena of an 18% thick biconvex airfoil in Xiao et al.,[31] and the predicted oscillation frequency is close to both experiments and other computations. The authors are not aware of other computational results of buffet for the BGK No. 1 airfoil. Further investigations into the quantitative agreement of the computed buffet frequency with experimental value are needed in future work.

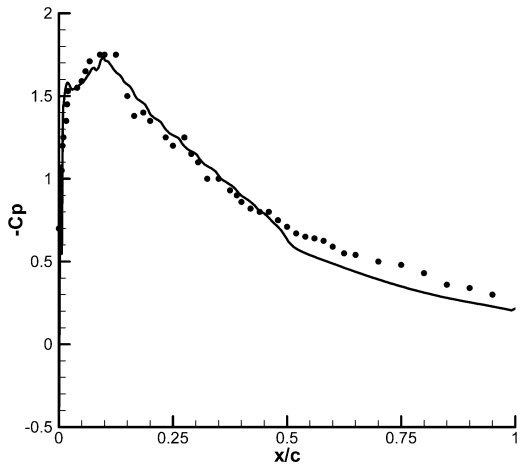

Fig. 7 Time-mean pressure distribution on the upper surface of wall comparison with experimental results: ●, experiment and ——, computation.

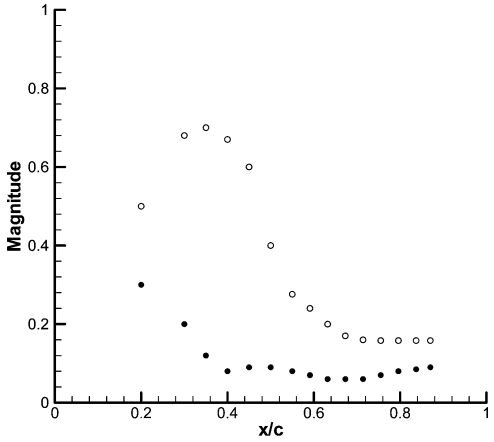

Fig. 8 Magnitude of pressure wave propagating: ●, experiment and ○, computation.

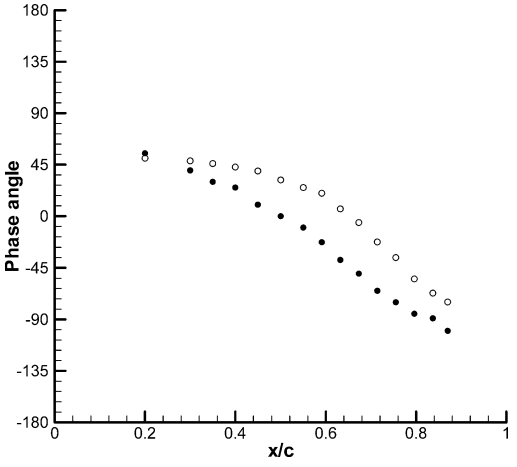

Fig. 9 Phase angle of pressure wave propagating: ●, experiment and ○, computation.

The time-mean pressure distribution along the upper surface of the wall is shown in Fig. 7 along with the experimental data of Lee. The computation is in good agreement with the experiment without angle-of-attack correction.

The magnitude and phase angle (relative to the shock oscillation) of the unsteady pressure at the E-T locations of the airfoil shown in Fig. 1 (obtained by FFT of –Cp) are presented in Figs. 8 and 9, respectively. The computations show an increase in amplitude with increasing x/c for $x/c < 0.4$, followed by a decrease within the range of $0.4 < x/c < 0.6$, and then almost constant values. The

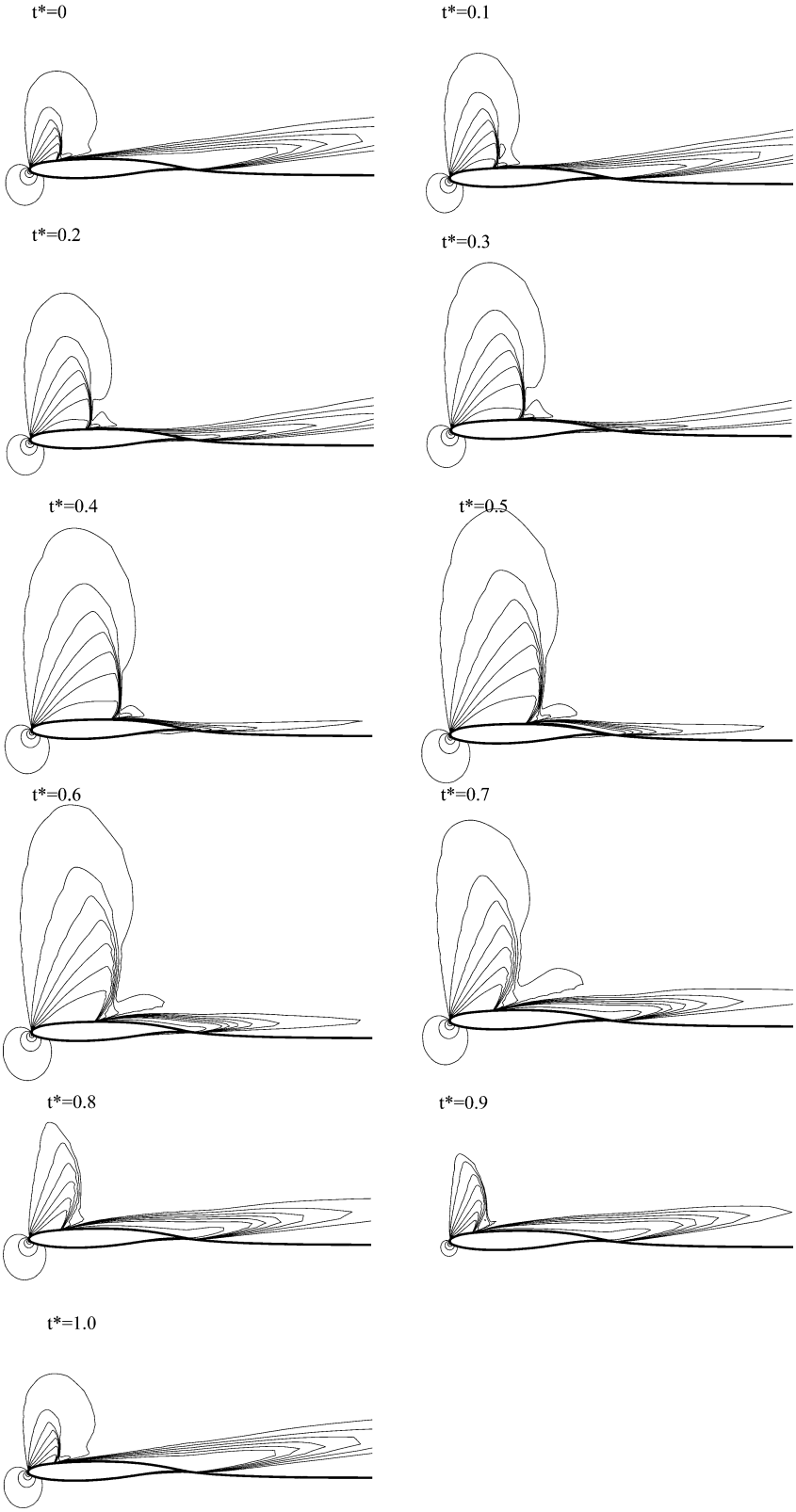

Fig. 10 Mach-number contour at different instant time in one period: $M = 0.71$ and $\alpha = 6.97$ deg; $\Delta M = 0.095$.

experiment, however, shows a continuous decrease of amplitude before $x/c < 0.4$ and then a slight increase and a decrease with x/c.

Although there exist large differences of amplitude between the experiment and computation, the agreement of the phase angle is much better, as shown in Fig. 9. An important feature to notice is that both results show a linear relationship between phase angle and the streamwise location after $x/c > 0.5$. This suggests a traveling pressure wave with a constant wave speed downstream of shock wave.

The origin and mechanism of self-excited oscillation in buffeting phenomena are not fully understood. A variety of concepts are discussed in the literature, for example, mechanisms related to the maximum Mach number ahead of the shock and the separation bubble,[17,18] and signal propagation in inner and outer separated flow regions.[11] We analyze our computational results to give insight into the oscillation physics by examining the motion of the shock, its concomitant evolution of the separation

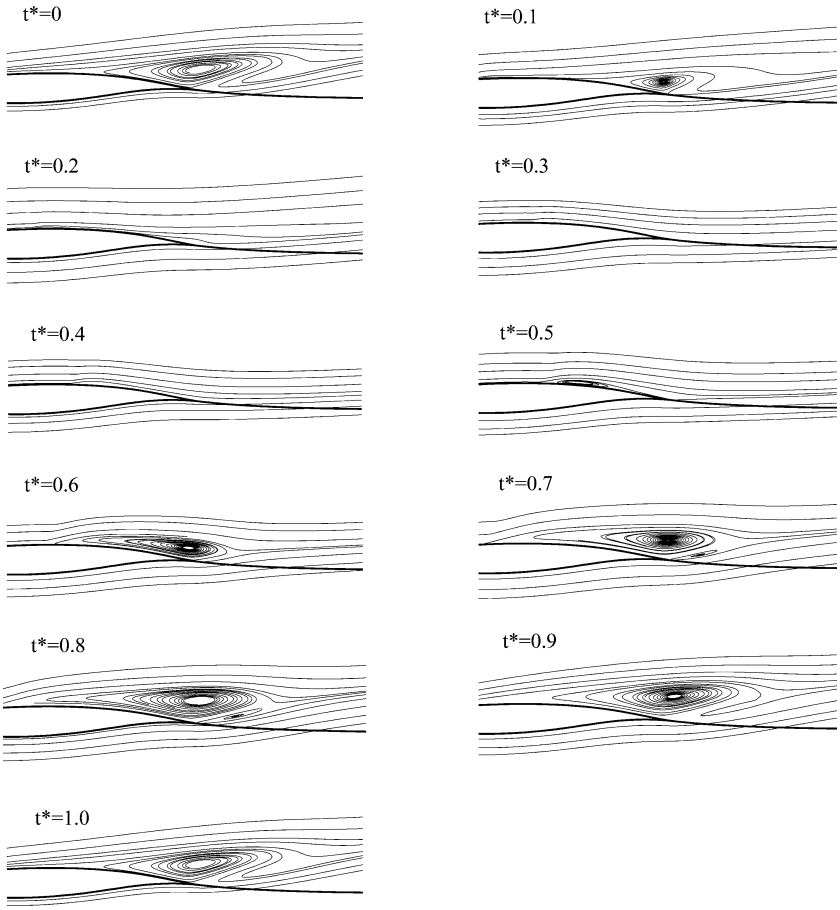

Fig. 11 Streamline plots at different instant time in one period: $M = 0.71$ and $\alpha = 6.97$ deg.

bubble, and the signal propagation path of the unsteady pressure disturbances.

The Mach-number contours and streamline plots near the trailing edge at different time instants during one oscillation cycle are shown in Figs. 10 and 11. The $t^* = 0$ corresponds to the time instant at which the lift coefficient Cl is the minimum, and $t^* = 1$ instant represents one completed cycle. Unlike in the case of the nonlifting biconvex circular-arc airfoil, the shock oscillation here occurs on the upper side of the airfoil only. The shock motion is mainly of the type A reported by Tijdeman.[32] As seen from both figures, at $t^* = 0$, a shock occurs at a location of approximately one-quarter chord of the airfoil, and there is a large separation region extending from $x/c = 0.65$ downstream to $x/c = 1.35$ in the wake region. At subsequent time instants, the shock becomes stronger and moves downstream, and the separated flow convects downstream and eventually disappears on the top region of the airfoil about the time from $t^* = 0.1$ to 0.2. At a later time separated flow reappears, and a bulge can be observed around $x/c = 0.55$ at $t^* = 0.3$, which then forms a new vortex. At the time instants of $t^* = 0.4$ and 0.5, the bulge becomes larger, and a large separation region appears at $t^* = 0.5$. This also corresponds to the instants of maximum lift. The shock reaches the most rearward position at about $t^* = 0.5$, which is followed by a forward movement of the shock in the second half of the cycle ($0.5 < t^* < 1.0$). The shock strength, however, continues to decrease during this period, which is indicated from the change of normal shock at $t^* = 0.4$ to oblique shock at $t^* = 0.8$. In the subsequent time instants ($t^* = 0.6$, 0.7, and 0.8), the vortex created at $t^* = 0.5$ increases its size in both upstream and downstream directions with a corresponding loss of lift. A secondary vortex is also formed in the vicinity of the trailing edge at $t^* = 0.7$ and 0.8. The vortices coalesce and form one large separation region, which decreases in size in the successive time instants $t^* = 0.9$ and 1.0. The cycle of separated flow and shock movement then repeats itself.

The upper wall pressure distribution at different time instants during one period is shown in Figs. 12a and 12b for the downward and upward movements of the shock. The shock motion is clearly seen, and large boundary-layer separation as a result of shock/boundary-layer interaction occurs near $t^* = 0$. The extension of the separation region is also time dependent.

Clearly the shock motion and the evolution of the shock-induced separation are intimately connected. Nevertheless, the cause-and-effect relation of the two is not clear. In addition, this phenomenological description does not yield information about the buffet frequency.

Lee[11,12] and Lee et al.[13] give an explanation of the mechanism of self-sustained shock oscillation and a method to estimate the frequency of oscillation. The model assumes that the flow behind the shock-boundary-layer interaction to be fully separated. The movement of the shock creates pressure waves, which propagate downstream in the separated flow region (Fig. 13). On reaching the trailing edge, the disturbances generate upstream-moving waves in the region outside the separated flow as a result of satisfying the unsteady "Kutta" condition. The upstream-moving wave interacts with the shock and imparts energy to return the shock to its initial location. The loop is then completed. The period of the shock oscillation is the time it takes for a disturbance to propagate from the shock to the trailing edge plus the duration for an upstream wave to reach the shock from the trailing edge. This is given by the following formulation[11]:

$$T_p = T_{p1} + T_{p2} \tag{15}$$

$$T_{p1} = \int_{x_s}^{c} \frac{1}{a_p}\,\mathrm{d}x \tag{16}$$

$$T_{p2} = -\int_{c}^{x_s} \frac{1}{a_u}\,\mathrm{d}x \tag{17}$$

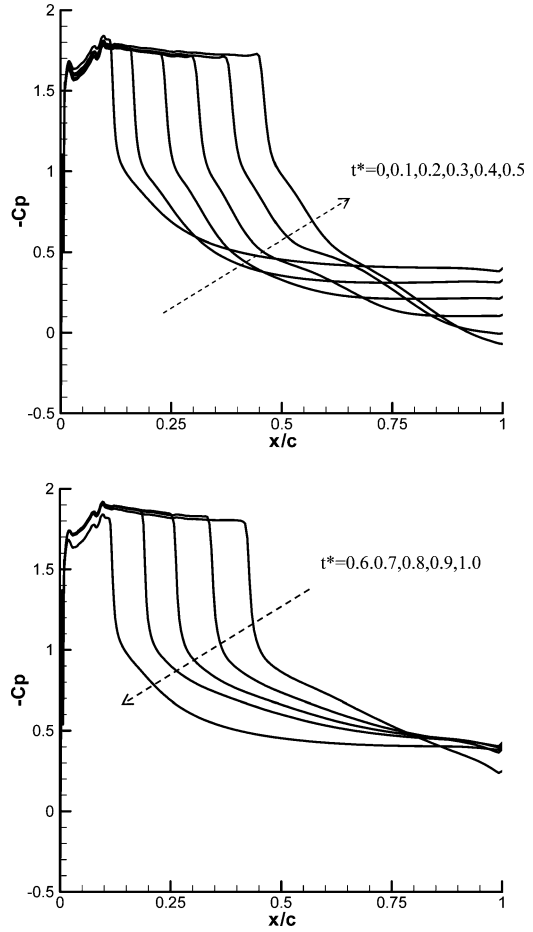

Fig. 12 Unsteady shock movement during one period.

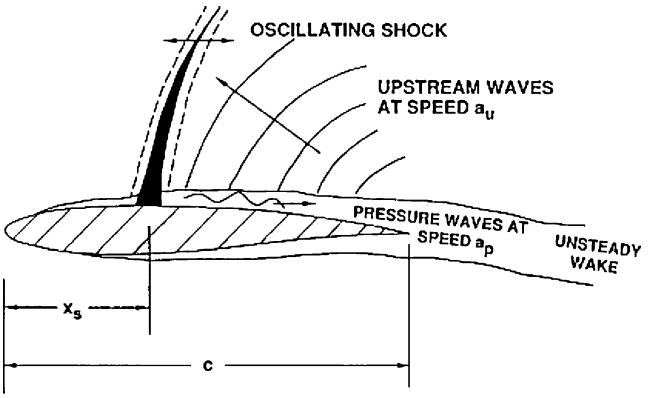

Fig. 13 Model of self-sustained oscillation (from Ref. 12).

where T_{p1} and a_p are the time and speed for the downstream pressure wave propagation; T_{p2} and a_u are the time and speed for the upstream wave, respectively; and x_s is the time-mean shock location. Various empirical formulas have been proposed by Lee,[11] Tijdeman,[32] Erickson and Stephenson,[33] Mabey,[34] and Mabey et al.[35] to estimate a_p and a_u or T_{p1} and T_{p2} based on the estimations of local Mach number and speed of sound.

In the present study, this empiricism can be avoided because we have the complete unsteady flowfield from the computation. Two-point cross correlation of the unsteady pressure is used to determine the propagation direction and speed of the pressure fluctuations along a given path. Within the separated region, the cross-correlation analysis is conducted for the points E to T (shown in Fig. 1) along the upper airfoil surface. Point T near the trailing edge is used as the reference point. A cross-correlation coefficient $R(x, y, \tau)$ for two variables x and y with time delay τ can be defined as

$$R(x, y, \tau) = \frac{\overline{x'(t)y'(t-\tau)}}{\overline{x'^2 y'^2}} \tag{18}$$

where x and y are the pressure fluctuations at the two points, and $x'(t)$ and $y'(t)$ are the fluctuating parts of x and y, respectively. The overbar stands for time averaging, for example,

$$\bar{x} = \lim_{T\to\infty}\left(\frac{1}{T}\right)\int_0^T x(t)\,\mathrm{d}t$$

Thus, we have

$$x(t) = \bar{x} + x'(t), \qquad y(t) = \bar{y} + y'(t)$$

In practice, because we have limited signal length, we use the cross-covariance function $x\mathrm{cov}(x, y)$ in MATLAB® to calculate $R(x, y, \tau)$. The results are shown in Fig. 14, where the positive time delays obtained in Fig. 14 indicate that the pressure disturbances within the separated region behind the shock waves propagate downstream toward the airfoil trailing edge. This is consistent with the phase-angle distribution of the unsteady pressure on the airfoil surface shown in Fig. 9. The local propagation speed of the pressure disturbances can be calculated by dividing the spatial distances between the neighboring points of pressure measurement by the time delays between the peaks of the corresponding cross correlations shown in Fig. 14. The total time for a disturbance from the shock wave to reach the airfoil trailing edge can then be integrated by using Eq. (16). The time-mean shock position x_s is 0.15 for this test case. Alternatively, a_p can also be calculated by using the phase delay between the points on the airfoil surface shown in Fig. 9. The almost linear relation of the phase angles shown in Fig. 9 for $x/c > 0.25$ indicates a near-constant wave speed, which for this case is about $0.12U_\infty$.

Outside the separation region, pressure correlations are formed along three different paths consisting of different selections of four points A, B, C, and D, as indicated in Table 1. Point A is fixed at the airfoil trailing edge for all of the three paths and is used

Table 1 Coordinates of off-body locations for cross-correlation analysis

Path	Coordinate	A	B	C	D
1	x/c	1.0	0.795	0.591	0.5
	y/c	0	0.0873	0.118	0.125
2	x/c	1.0	0.795	0.591	0.5
	y/c	0	0.112	0.136	0.138
3	x/c	1.0	0.795	0.591	0.5
	y/c	0	0.126	0.157	0.157

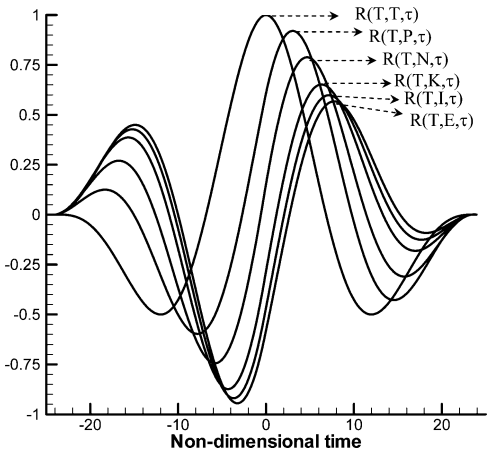

Fig. 14 Cross correlation of the downstream pressure wave inside the separation region.

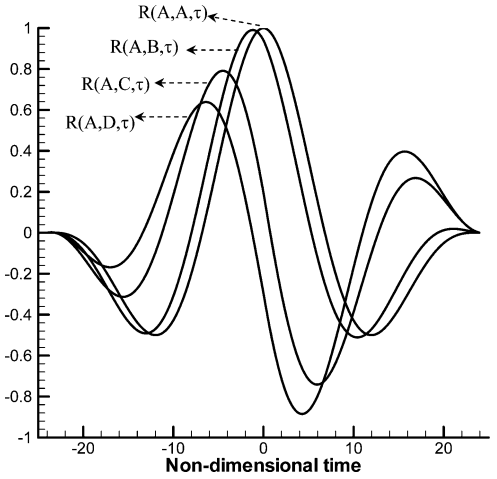

Fig. 15 Cross correlation of upstream wave.

as the reference point for all of the cross correlations. The cross-correlation results are shown in Fig. 15. The negative time delays of the successive points relative to each other indicate that the unsteady disturbances propagate upstream from point A to point D. This is in complete agreement with the hypothesis of Lee's signal propagation model. Results on the other two paths outside the separation region show the same trends but with slightly different time delays between peaks. The local wave speed of this upstream propagation can again be calculated by dividing the spatial distances between the points A, B, C, and D and the corresponding time delays in the pressure correlations. The upstream propagation time T_{p2} is then computed by integration Eq. (17) along the path of A to D. The times so calculated for the three paths shown in Table 1 are slightly different. Integration along path 1 yields the shortest time. Lee[11] reported the existence of a maximum initial ray angle within which a disturbance generated at the trailing edge can reach the shock wave. This angle is called critical ray angle. The minimum propagation time T_{p2} is the time it takes a disturbance to travel from the source located at the trailing edge to the shock wave along this critical ray. Our computations indicate path 1 is close to the critical ray for this test case.

It is shown from Fig. 14 that, inside the separated region, the pressure disturbances propagate downstream from shock to the trailing edge. However, negative time delay is observed in Fig. 15 for the pressure outside the separation region, which indicates that the disturbances are moving upstream. Lee's signal propagation model[11] suggests that the period of buffet is the sum of T_{p1} and T_{p2}, from which the reduced frequency ($k = \pi f c / U_\infty$) of buffet can be calculated, where $f = 1/T_p$. For this test case we obtain $k = 0.175$. The FFT of the computed lift coefficient gives $k = 0.16$. This excellent agreement of the computed buffet frequency with that obtained from the signal propagation hypothesis using the computational data lends strong support for the mechanism of self-sustained oscillation proposed by Lee.

Case 3 ($M = 0.71$, $\alpha = 9.0$ deg)

Time-accurate computation of this case is performed starting from the uniform freestream flow. The computed history of lift coefficient shows the flow becomes steady again. The final steady-state Mach-number contours and top wall pressure distribution show that the shock is near the leading edge and a strong separation extends to the trailing edge. The details of the computational results are omitted here.

Conclusions

The unsteady Reynolds-averaged Navier–Stokes computation of the self-excited oscillation on the BGK No. 1 supercritical airfoil is conducted using the lagged two-equation k–ω turbulence model. Pressure correlations of the computed unsteady flowfield are used to calculate the signal propagation direction and speed within and outside the separation region between the shock and the airfoil trailing edge. Results confirm that pressure waves behind the shock propagate downstream within the separated region. On reaching the trailing edge, the disturbances generate upstream-moving wave outside of the separated region. The period of the shock oscillation estimated as the total time for a disturbance to make such a round-trip travel agrees well with that obtained directly from the Fourier analysis of the computed lift coefficient, providing strong support for the buffet model proposed by Lee[11] based on a signal propagation mechanism.

Acknowledgment

We thank B.K.H. Lee of the National Research Council, Canada, for providing us the necessary data from his experimental work.

References

[1]McDevitt, J. B., Levy, L. L., and Deiwert, G. S., "Transonic Flow About a Thick Circular-Arc Airfoil," *AIAA Journal*, Vol. 14, No. 5, 1976, pp. 606–613.

[2]Levy, L. L., "Experimental and Computational Steady and Unsteady Transonic Flows About a Thick Airfoil," *AIAA Journal*, Vol. 16, No. 6, 1978, pp. 564–572.

[3]Rumsey, C. L., Sanetrik, M. D., Biedron, R. T., Melson, N. D., and Parlette, E. B., "Efficiency and Accuracy of Time-Accurate Turbulent Navier–Stokes Computation," *Computers and Fluids*, Vol. 25, No. 2, 1996, pp. 217–236.

[4]Edwards, J. W., "Transonic Shock Oscillations Calculated with a New Interactive Boundary Layer Coupling Method," AIAA Paper 93-0777, 1993.

[5]Oliver, R., Stylvie, P., and Vincent, C., "Numerical Simulation of Buffeting over Airfoil Using Dual Time-Stepping Method," European Congress on Computational Methods in Applied Science and Engineering, Sept. 2000.

[6]Barakos, G., and Drikakis, D., "Numerical Simulation of Transonic Buffet Flows Using Various Turbulence Closures," *International Journal of Heat and Fluid Flow*, Vol. 21, No. 5, 2000, pp. 620–626.

[7]Bartels, R. E., "Flow and Turbulence Modeling and Computation of Shock Buffet Onset for Conventional and Supercritical Airfoils," NASA TP-1998-206908, Feb. 1998.

[8]Bartels, R. E., and Edwards, J. W., "Cryogenic Tunnel Pressure Measurements on a Supercritical Airfoil for Several Shock Buffet Conditions," NASA TM-110272, 1997.

[9]Lee, B. H. K., "Transonic Buffet on a Supercritical Airfoil," *Aeronautic Journal*, Vol. 94, No. 935, 1990, pp. 143–152.

[10]Lee, B. H. K., Ellis, F. A., and Bureau, J., "Investigation of the Buffet Characteristics of Two Supercritical Airfoils," *Journal of Aircraft*, Vol. 26, No. 8, 1989, pp. 731–736.

[11]Lee, B. H. K., "Oscillation Shock Motion Caused by Transonic Shock Boundary Layer Interaction," *AIAA Journal*, Vol. 28, No. 5, 1990, pp. 942–944.

[12]Lee, B. H. K., "Self-Sustained Shock Oscillations on Airfoils at Transonic Speeds," *Progress in Aerospace Sciences*, Vol. 37, No. 2, 2001, pp. 147–196.

[13]Lee, B. H. K., Murty, H., and Jiang, H., "Role of Kutta Waves on Oscillatory Shock Motion on an Airfoil," *AIAA Journal*, Vol. 32, No. 4, 1994, pp. 789–795.

[14]Girodroux-Lavigne, P., and LeBalleur, J. C., "Time Consistent Computation of Transonic Buffet over Airfoils," *Proceedings of the 16th Congress of the International Council of the Aeronautical Sciences*, 1988, pp. 779–787.

[15]Mabey, D. G., "Physical Phenomena Associated with Unsteady Transonic Flow," *Unsteady Transonic Aerodynamics*, edited by D. Nixon, Vol. 120, Progress in Aeronautics and Astronautics, AIAA, Washington, DC, 1989, Chap. 1.

[16]Raghunathan, S., Hall, D. E., and Mabey, D. G., "Alleviation of Shock Oscillations in Transonic Flow by Passive Control," *Aeronautical Journal*, Vol. 94, No. 937, 1990, pp. 245–250.

[17]Raghunathan, S., Mitchell, R. D., and Gillan, M. A., "Transonic Shock Oscillations on NACA0012 Aerofoil," *Shock Waves*, Vol. 8, No. 4, 1998, pp. 191–202.

[18]Raghunathan, S., Gillan, M. A., Cooper, R. K., Mitchell, R. D., and Cole, J. S., "Shock Oscillations on Biconvex Aerofoils," *Aerospace Science and Technology*, Vol. 3, No. 1, 1999, pp. 1–9.

[19]Gibb, J., "The Cause and Cure of Periodic Flows at Transonic Speeds," *Proceedings of the 16th Congress of the International Council of the Aeronautical Sciences*, 1988, pp. 1522–1530.

[20]Xiao, Q., Tsai, H. M., and Liu, F., "Computation of Transonic Diffuser Flows by a Lagged k–ω Turbulence Model," *Journal of Propulsion and Power*, Vol. 19, No. 3, 2003, pp. 473–483.

[21]Xiao, Q., Tsai, H. M., and Liu, F., "Computation of Turbulent Separated Nozzle Flow by a Lag Model," *Journal of Propulsion and Power*, Vol. 21, No. 2, 2005, pp. 368–371.

[22]Olsen, M. E., and Coakley, T. J., "The Lag Model, a Turbulence Model for Nonequilibrium Flows," AIAA Paper 2001-2564, 2001.

[23]Baldwin, B. S., and Lomax, H., "Thin Layer Approximation and Algebraic Model for Separated Turbulent Flows," AIAA Paper 78-257, 1978.

[24]Spalart, P. R., and Allmaras, S. R., "A One-Equation Turbulence Model for Aerodynamic Flows," AIAA Paper 92-0439, 1992.

[25]Launder, B. E., and Sharma, B. I., "Application of the Energy-Dissipation Model of Turbulence to the Calculation of Flow near a Spinning Disk," *Letters in Heat and Mass Transfer*, Vol. 1, No. 2, 1974, pp. 131–138.

[26]Nagano, Y., and Kim, C., "A Two Equation Model for Heat Transport in Wall Turbulent Shear Flows," *Journal of Heat Transfer*, Vol. 110, No. 3, 1988, pp. 583–589.

[27]Craft, T. J., Launder, B. E., and Suga, K., "Development and Application of a Cubic Eddy-Viscosity Model of Turbulence," *International Journal of Heat and Fluid Flow*, Vol. 17, No. 2, 1996, pp. 108–115.

[28]Sofialidis, D., and Prinos, P., "Development of a Non-Linear Strain Sensitive k–ω Turbulence Model," *Proceedings of the 11th Symposium on Turbulent Shear Flows, TSF-11*, 1997, pp. 2-89–2-94.

[29]Liu, F., and Ji, S., "Unsteady Flow Calculations with a Multigrid Navier–Stokes Method," *AIAA Journal*, Vol. 34, No. 10, 1996, pp. 2047–2053.

[30]Jameson, A., "Transonic Flow Calculations," Dept. of Mechanical and Aerospace Engineering, MAE Rept. 1651, Princeton Univ., Princeton, NJ, July 1983.

[31]Xiao, Q., Tsai, H. M., and Liu, F., "Computation of Shock Induced Separated Flow with a Lagged k–ω Turbulence Model," AIAA Paper 2003-3464, 2003.

[32]Tijdeman, H., "Investigation of the Transonic Flow Around Oscillation Airfoils," National Aerospace Lab., NLR TR 77090 U, The Netherlands, Dec. 1977.

[33]Erickson, A. L., and Stephenson, J. D., "A Suggested Method of Analyzing Transonic Flutter of Control Surfaces Based on Available Experimental Evidence," NACA RM A7F30, Dec. 1947.

[34]Mabey, D. G., "Oscillatory Flows from Shock-Induced Separations on Biconvex Airfoils of Varying Thickness in Ventilated Wind Tunnels," AGARD CP-296, *Boundary Layer Effects on Unsteady Airfoils*, 1980, pp. 11.1–14.

[35]Mabey, D. G., Welsh, B. L., and Cripps, B. E., "Periodic Flows on a Rigid 14% Thick Biconvex Wing at Transonic Speeds," Royal Aircraft Establishment, TR81059, Bedford, England, U.K., May 1981.

S. Mahalingam
Associate Editor